

# IRAK1/4/pan-FLT3 Kinase Inhibitors with Reduced hERG Block as Treatments for Acute Myeloid Leukemia

Scott B. Hoyt,\* Chris J. Finocchio, Elizabeth Croll, Gregory J. Tawa, Mingliang Zhang, Jiangong Wang, Huixi Li, Li Ma, Kaikai Li, Xiaohu Zhang, Xin Xu, Pranav Shah, Yuhong Fang, Lyndsey C. Bolanos, Gabriel Gracia-Maldonado, Amal Kolt, Christina Robinson, Jessica Free, Elijah F. Edmondson, Simone Difilippantonio, LaQuita M. Jones, Ashley E. Culver-Cochran, Jan S. Rosenbaum, Daniel T. Starczynowski, and Craig J. Thomas

Cite This: *ACS Med. Chem. Lett.* 2025, 16, 887–895

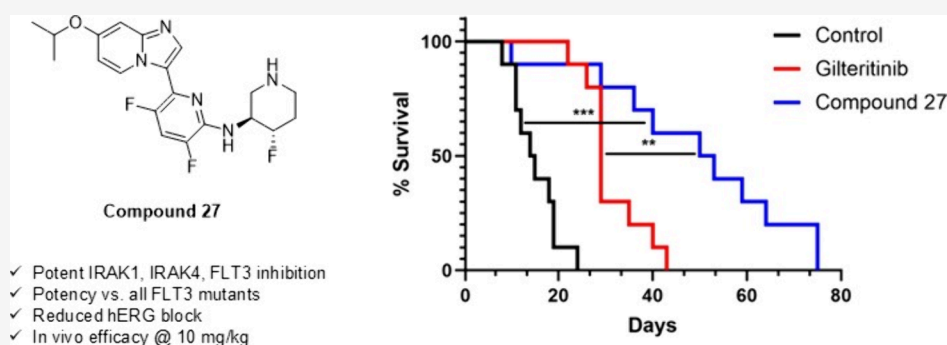
Read Online

ACCESS |

Metrics & More

Article Recommendations

Supporting Information



**ABSTRACT:** We report the optimization of a series of IRAK1/4/pan-FLT3 kinase inhibitors. These efforts have produced a key compound 27 that displays potent and selective inhibition of IRAK1, IRAK4, and FLT3, reduced block of hERG, and good pharmacokinetic properties. In a mouse xenograft model of acute myeloid leukemia (AML), 27 produces survival prolongation superior to that of gilteritinib, the leading FDA-approved FLT3 inhibitor currently used to treat AML.

**KEYWORDS:** IRAK1, IRAK4, FLT3, kinase, AML, leukemia

Acute myeloid leukemia (AML) is an aggressive blood cell cancer that is currently not well treated.<sup>1</sup> Existing therapies include classical chemotherapeutic agents, FLT3 kinase inhibitors, and, for patients healthy enough to withstand the procedure, hematopoietic stem cell transplantation.<sup>2</sup> Even with those options, however, the prognosis for AML patients is often poor, with most surviving only a few years postdiagnosis.<sup>3</sup>

FLT3 is a receptor tyrosine kinase that can initiate signaling through multiple pathways associated with cell growth and proliferation.<sup>4</sup> In AML, a variety of FLT3 mutations can produce constitutive activation of the kinase and its downstream signaling pathways.<sup>5</sup> That aberrant, unchecked signaling promotes the rapid growth and proliferation of AML tumor cells, and is a key driver of disease progression.<sup>6</sup>

Significant efforts have been directed toward the discovery of FLT3 inhibitors as treatments for AML.<sup>7</sup> These efforts have culminated in FDA approval of three agents to date: midostaurin, a first-generation inhibitor of FLT3 and other kinases, as well as gilteritinib and quizartinib, more selective second-generation inhibitors (Figure 1). Treatment of AML patients with these inhibitors can produce promising initial response rates. However, for many patients durable remission

proves elusive, in part because of the emergence of adaptive signaling pathways that circumvent the effects of the inhibitors.

Recent work has established the importance of IRAK-mediated signaling as a critical adaptive resistance pathway that emerges in AML.<sup>8</sup> In patients treated with a FLT3 inhibitor, signaling through the FLT3-mediated pathway is effectively blocked, but compensatory signaling through IRAK1 and IRAK4 is upregulated. This adaptive signaling promotes the continued growth and proliferation of the cancer. Selective knockdown or inhibition of IRAK4 can attenuate signaling through this pathway. However, to maximize block of signaling and antileukemic efficacy in cell or mouse models of AML, knockdown or inhibition of both IRAK1 and IRAK4 is required.<sup>9</sup>

Received: March 18, 2025

Revised: April 22, 2025

Accepted: April 23, 2025

Published: April 29, 2025



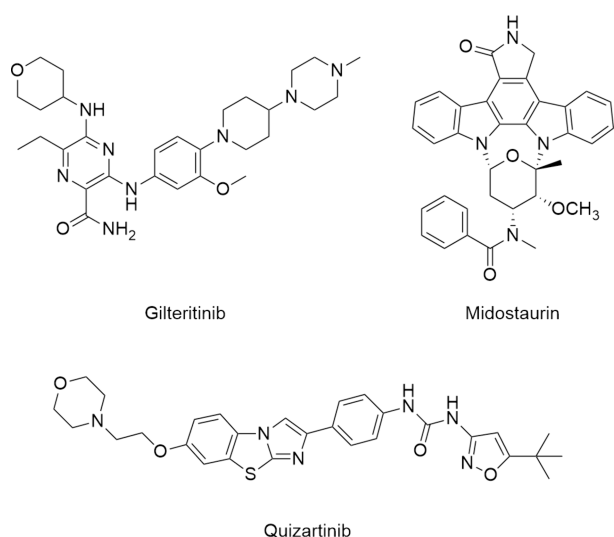


**Figure 1.** FDA-approved FLT3 inhibitors.

Our goal is to discover compounds that potently and selectively inhibit IRAK1, IRAK4, FLT3, and key mutant forms of FLT3. These agents should effectively block signaling through both the IRAK- and FLT3-mediated pathways, and should thus offer improved efficacy relative to the FLT3 inhibitors that have advanced previously into the clinic as treatments for AML.

Prior work in this series led to the identification of compounds such as **1** (Figure 2) that displayed potent and selective inhibition of IRAK1, IRAK4, and FLT3.<sup>10</sup> Unfortunately, many of these earlier compounds also exhibited block of hERG, a voltage-gated potassium channel that is critical for normal cardiac functioning.

The pharmacophore of compounds that block hERG is known, and is embodied in compounds such as **1**.<sup>11</sup> As noted in a recent review, compounds that potently block hERG typically contain a centrally located basic amine connected to several lipophilic aromatic groups.<sup>12</sup> In the Pearlstein variant of the pharmacophore, one of those aromatic groups may be replaced by a polar ‘tail’. Compound **1** and other early compounds in this series all contain key features of the Pearlstein pharmacophore: a centrally located 2-aminopyridine ( $pK_a \sim 6.9$ , highlighted in red) connected to an aromatic group (the bicyclic imidazopyridine, in yellow) and a polar tail (the pyrrolidine, in green). Perhaps not surprisingly, compound **1** displays moderately potent hERG block ( $IC_{50} = 0.9 \mu M$ ) as measured in a manual patch-clamp assay (Figure 2).

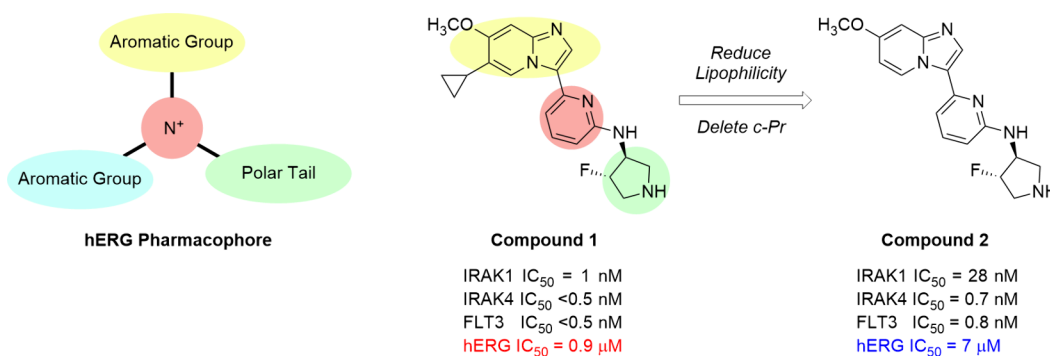


**Figure 2.** The Pearlstein hERG pharmacophore informs strategies for hERG reduction.

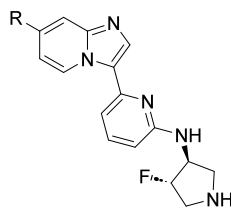
Problematically, each of the substructures that putatively contribute to hERG block also appeared, based on prior SAR, to be essential for on-target potency.<sup>10</sup> It was thus clear that reduction of hERG in this series would require judicious modification of these structures.

Working within those constraints, we endeavored to reduce hERG block while maintaining potent inhibition of our key targets. Toward that end, we initially attempted to reduce the lipophilicity of the hinge-binding imidazopyridine by deleting the C6-cyclopropyl group of **1** to afford compound **2** (Figure 2). That excision delivered a nearly 10-fold reduction in hERG potency while preserving potent inhibition of IRAK1, IRAK4 and FLT3. Encouraged by these results, we sought to further explore the potential of this C6–H series.

We began our SAR studies by examining the effects of substitution at the imidazopyridine C7 position. As shown in Table 1, the parent unsubstituted compound in this series (compound **3**) displayed moderate inhibition of IRAK1, as well as more potent inhibition of IRAK4 and FLT3. Substitution at C7 with fluorine (compound **4**) proved detrimental to IRAK1 and IRAK4 inhibition. In contrast, substitution with chlorine (compound **5**) or, even better, cyclopropyl (compound **6**) afforded improved IRAK1 and IRAK4 inhibition. Since cyclopropyl substitution appeared beneficial, we also prepared methylcyclopropyl and trifluoromethylcyclopropyl analogs **7** and **8**. Unfortunately, as the steric bulk of the cyclopropyl moiety increased, IRAK inhibitory potencies decreased. In contrast to the results obtained with compound **4**, substitution at C7 with an electron-donating methoxy group (compound **2**) imparted improved IRAK1 and IRAK4 inhibition relative to unsubstituted parent **3**. As compound **2** exhibited reduced stability in rat liver microsome (RLM) incubations, we prepared a variety of C7-fluoroalkoxy analogs (compounds **9–11**), as well as several bulkier alkoxy derivatives (compounds **12** and **13**), in an attempt to block any oxidative metabolism that might be occurring at the ether methyl group. Notably, compounds **9–13** all displayed improved stability in RLM incubations relative to methoxy analog **2**. Of the three fluoroalkoxy analogs, compounds **9** and **11**, which contained less electron-withdrawing difluoromethoxy and difluoroethoxy groups, exhibited improved IRAK4 inhibition relative to trifluoromethoxy derivative **10**.

We also examined the effect of incorporating polar functional groups at C7. These groups could conceivably disrupt bonding interactions between the imidazopyridine and the aromatic side chains that line the hERG channel pore, thereby affording reduced hERG block. To test this hypothesis, we synthesized

Table 1. Effect of C7 Substitution on Potency and In Vitro ADME Properties



| Compd | R                                  | IRAK1 IC <sub>50</sub> (nM) <sup>a</sup> | IRAK4 IC <sub>50</sub> (nM) <sup>a</sup> | FLT3 IC <sub>50</sub> (nM) <sup>a</sup> | PAMPA (P <sub>app</sub> ) <sup>b</sup> | RLM t <sub>1/2</sub> (min) <sup>c</sup> |
|-------|------------------------------------|--|--|---|--|---|
| 3     | H                                  | 212                                      | 7  | <0.5                                    | 1115                                   | 89                                      |
| 4     | F                                  | 1540 <sup>d</sup>                        | 37 <sup>d</sup>                          | 1 <sup>d</sup>                          | 1223                                   | 82                                      |
| 5     | Cl                                 | 82                                       | 3  | 0.6                                     | 1310                                   | 79                                      |
| 6     | <i>c</i> -Pr                       | 6  | 2  | <0.5                                    | N.D.                                   | 51                                      |
| 7     |                                    | 45                                       | 2  | <0.5                                    | 993                                    | 37                                      |
| 8     |                                    | 2137                                     | 418                                      | 0.7                                     | 1144                                   | 30                                      |
| 2     | OCH <sub>3</sub>                   | 20                                       | 0.6                                      | 0.6                                     | 412                                    | 24                                      |
| 9     | OCF <sub>2</sub> H                 | 25                                       | 2  | <0.5                                    | 1009                                   | 107                                     |
| 10    | OCF <sub>3</sub>                   | 75                                       | 38                                       | 1                                       | 1016                                   | 102                                     |
| 11    | OCH <sub>2</sub> CF <sub>2</sub> H | 31                                       | 0.6                                      | <0.5                                    | N.D.                                   | 51                                      |
| 12    | <i>O</i> - <i>i</i> -Pr            | 15                                       | 0.9                                      | <0.5                                    | 848                                    | 59                                      |
| 13    | <i>O</i> - <i>c</i> -Pr            | 18                                       | 0.9                                      | <0.5                                    | 1288                                   | 63                                      |

<sup>a</sup>Data are the geometric mean of two independent experiments ( $n = 2$ ) unless otherwise specified. Assay details reported in [Supporting Information](#). <sup>b</sup>Permeability ( $P_{app} \times 10^{-6}$  cm/s) as measured in PAMPA assay. <sup>c</sup>Half-life of compound incubated with rat liver microsomes (RLM). <sup>d</sup>Data are from a single experiment ( $n = 1$ ).

amides 14–16. As shown in [Table 2](#), primary amide 14 and methyl amide 15 displayed potent inhibition of IRAK4 and FLT3, and moderate inhibition of IRAK1. In contrast, dimethyl amide 16 proved much less potent.

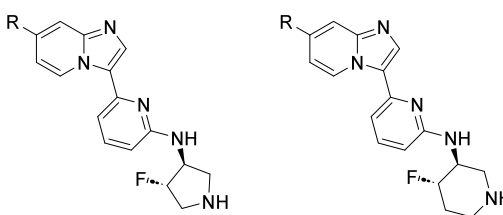
Pyrrolidine amides 14 and 15 offered reasonable potency profiles, but suffered from poor permeability.<sup>13</sup> We had previously observed that the permeabilities of analogous piperidine derivatives were often higher than those of the corresponding pyrrolidines.<sup>10</sup> We thus prepared piperidine methyl amide 17, but were disappointed to see that it exhibited low permeability comparable to that of pyrrolidine methyl amide 15. Attempting to further improve permeability in this series, we synthesized a large set of derivatives wherein the amide R group was varied. Isopropyl amide 18 serves as a representative example from this set, and illustrates that variation in the amide R group afforded, at best, only modest permeability enhancement. Finally, a variety of compounds containing heterocyclic amide isosteres were also prepared. As shown in [Table 2](#), imidazole 19 and triazole 20 displayed potencies and ADME properties similar to those of their amide counterparts. In contrast, regioisomeric imidazole 21 and triazole 22 evinced greatly improved IRAK1 inhibition. Unfortunately, like other compounds in this series, they suffered from low permeability. Various strategies to improve permeability by modifying other parts of the molecule were unsuccessful, and as a result, it ultimately proved difficult to incorporate these polar C7 groups into more advanced analogs.

With substitution at C7 optimized, we next examined modifications of the central pyridine ring, focusing on those that could potentially reduce hERG block. As shown in [Table 3](#), the parent compound in this series (compound 23) displayed potent inhibition of IRAK1, IRAK4, and FLT3, high permeability and metabolic stability, and moderate hERG

block as measured in a manual patch-clamp assay. The Pearlstein pharmacophore implicated the pyridine as a key feature contributing to hERG block. However, prior work had established that the pyridine and the 2-amino substituent that increased its basicity were both essential for potent IRAK and FLT3 inhibition.<sup>10</sup> With that in mind, we focused on modifications that would retain the pyridine or an isostere thereof while attenuating that ring's basicity. We began by substituting the pyridine with electron-withdrawing groups at the 3-, 4- and 5-positions. Early, as-yet-unpublished work in this series had shown that only small substituents such as hydrogen and fluorine were tolerated at these positions, and that incorporation of even slightly larger groups typically led to significant reductions in potency. We thus prioritized fluoro substitution, and synthesized monofluorinated analogs 24–26. Each of those exhibited IRAK and FLT3 potencies comparable to those of unsubstituted pyridine 23. Unfortunately, none of the monofluorinated analogs evinced significant reductions in hERG block. The 3,5-difluoropyridine derivative 27 was also prepared, and gratifyingly displayed potent IRAK1 inhibition as well as slightly reduced hERG block compared to 23.

Noting that the dual nature of fluorine (electron-withdrawing, but also lipophilicity-enhancing) made it an imperfect tool for hERG reduction, we next employed a different approach, one that would afford reductions in both basicity and lipophilicity. Toward that end we synthesized the pyrimidine and pyrazine analogs 28–30. As shown in [Table 3](#), there was a clear preference for location of the second ring nitrogen. Relative to pyridine 23, pyrimidine 28 displayed greatly reduced IRAK1 and IRAK4 inhibition. In contrast, pyrazine 29 and pyrimidine 30 offered potencies comparable to those of 23, while also affording modest reductions in hERG block. Thiazole and thiadiazole derivatives 31–33 were also prepared. Each of these

Table 2. Effect of C7 Substitution on Potency and In Vitro ADME Properties



| Compd | R   | IRAK1 IC <sub>50</sub> (nM) <sup>a</sup> | IRAK4 IC <sub>50</sub> (nM) <sup>a</sup> | FLT3 IC <sub>50</sub> (nM) <sup>a</sup> | PAMPA (P <sub>app</sub> ) <sup>b</sup> | RLM t <sub>1/2</sub> (min) <sup>c</sup> |
|-------|---|--|--|---|--|---|
| 14    |    | 158                                      | 2  | 0.7                                     | 1                                      | 66                                      |
| 15    |    | 126                                      | 1  | 0.5                                     | 2                                      | 49                                      |
| 16    |    | 2192                                     | 126                                      | 1                                       | <1                                     | 59                                      |
| 17    |    | 150                                      | 0.6                                      | <0.5                                    | 4                                      | >30                                     |
| 18    |    | 182                                      | 2  | <0.5                                    | 32                                     | 45                                      |
| 19    |    | 151                                      | 1  | <0.5                                    | 10                                     | 59                                      |
| 20    |   | 95                                       | 6  | 1                                       | N.D.                                   | >30                                     |
| 21    |  | 12                                       | 0.5                                      | <0.5                                    | 3                                      | N.D.                                    |
| 22    |  | 10                                       | <0.5                                     | <0.5                                    | <1                                     | 5                                       |

<sup>a</sup>Data are the geometric mean of two independent experiments ( $n = 2$ ) unless otherwise specified. Assay details reported in [Supporting Information](#). <sup>b</sup>Permeability ( $P_{app} \times 10^{-6}$  cm/s) as measured in PAMPA assay. <sup>c</sup>Half-life of compound incubated with rat liver microsomes (RLM).

less basic pyridine isosteres afforded moderate reductions in hERG block, but only thiadiazole **33** delivered acceptable IRAK inhibition. Finally, as thiadiazole **33** exhibited a promising profile, we synthesized the related oxadiazole **34**. While **34** provided the most effective hERG reduction in this series, it offered only weak inhibition of IRAK1, IRAK4, and FLT3. From this set, the difluoropyridine, pyrazine, pyrimidine, and thiadiazole cores imparted the best overall balance of properties, and were thus featured in a final round of SAR studies detailed below.

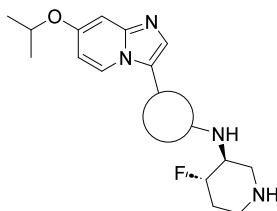
With optimal central rings identified, we made one final modification to the structure, and replaced the C7 isopropoxy group with a methoxy group to reduce lipophilicity and potentially further reduce hERG block. As shown in [Table 4](#), we prepared C7 methoxy derivatives that contained the 3,5-difluoropyridine, pyrazine, pyrimidine, and thiadiazole central cores (compounds **35–38**). Of these, compounds **35–37** maintained IRAK1, IRAK4, and FLT3 potencies comparable to or better than those observed with the corresponding C7 isopropoxy analogs. In contrast, compound **38** exhibited weaker IRAK1 inhibition than its C7 isopropoxy counterpart **33**. Compound **36** displayed a 3-fold reduction in hERG IC<sub>50</sub> relative to isopropoxy analog **29**, and in doing so exhibited the weakest hERG block we had observed in this series, a 20-fold reduction relative to starting point **1**. Compounds **35** and **37**, on

the other hand, showed no further reductions in hERG block relative to their isopropoxy counterparts. On the basis of the data presented above, compounds **27**, **30**, and **36** were judged to provide the best balance of potent on-target inhibition, reduced hERG block, and good in vitro ADME properties, and were thus selected for advanced profiling as described below.

Key compounds **27**, **30** and **36** displayed potent binding to IRAK1, IRAK4, FLT3, and clinically relevant FLT3 mutant isoforms (see [Supporting Information Table S7](#) for details).

Key compounds also exhibited potent activity across a variety of cell-based assays. As shown in [Table 5](#), compounds **27**, **30**, and **36** were tested in NanoBRET assays that measure IRAK4, FLT3, and FLT3 (D835Y) potencies in a cellular context. These assays allow potency to be measured versus the full-length kinase, and in the presence of physiological levels of ATP, partner proteins, and cofactors that might be absent in a biochemical assay. For these reasons, potencies determined in cellular NanoBRET assays are presumed to be more translatable to preclinical and clinical *in vivo* settings than those obtained from simpler biochemical assays. Compounds **27**, **30**, and **36** proved highly potent in the IRAK4, FLT3, and FLT3 (D835Y) NanoBRET assays, thus building confidence that the activities observed in earlier-stage biochemical assays would translate to *in vivo* efficacy.

Table 3. Effect of Central Ring on Potency, hERG, and In Vitro ADME Properties



| Compd | Central Ring | IRAK1<br>(nM) <sup>a</sup> | IC <sub>50</sub> | IRAK4<br>(nM) <sup>a</sup> | IC <sub>50</sub> | FLT3<br>(nM) <sup>a</sup> | IC <sub>50</sub> | hERG<br>(μM) <sup>a</sup> | IC <sub>50</sub> | PAMPA<br>(P <sub>app</sub> ) <sup>b</sup> | R/M/H<br>(min) <sup>d</sup> | LM<br>t <sub>1/2</sub> |
|-------|--------------|----------------------------|------------------|----------------------------|------------------|---------------------------|------------------|---------------------------|------------------|---|-----------------------------|------------------------|
| 23    |              | 23                         |                  | 2                          |                  | <0.5                      |                  | 2.9                       |                  | 1375                                      | >120 / 107 / >120           |                        |
| 24    |              | 7                          |                  | 0.7                        |                  | <0.5                      |                  | 3.6                       |                  | 1327                                      | 13 / 32 / 34                |                        |
| 25    |              | 12                         |                  | 2                          |                  | <0.5                      |                  | 1.4                       |                  | 1506                                      | 110 / 41 / 105              |                        |
| 26    |              | 16                         |                  | 1                          |                  | <0.5                      |                  | 4.1                       |                  | N.D.                                      | 48 / 18 / N.D.              |                        |
| 27    |              | 10                         |                  | 0.7                        |                  | <0.5                      |                  | 6.7                       |                  | 613                                       | 81 / 41 / 20                |                        |
| 28    |              | 768                        |                  | 30                         |                  | 0.6                       |                  | N.D.                      |                  | N.D.                                      | >120 / 17 / 39              |                        |
| 29    |              | 44                         |                  | 1                          |                  | <0.5                      |                  | 6.8                       |                  | 978                                       | 18 / 19 / 31                |                        |
| 30    |              | 10                         |                  | 0.9                        |                  | <0.5                      |                  | 5.1                       |                  | 1737                                      | 107 / N.D. / 65             |                        |
| 31    |              | 494                        |                  | 13                         |                  | 0.6                       |                  | 9.3                       |                  | N.D.                                      | 41 / 21 / 72                |                        |
| 32    |              | 2048                       |                  | 358                        |                  | 1                         |                  | 7.4                       |                  | N.D.                                      | 76 / 81 / 95                |                        |
| 33    |              | 14                         |                  | 7                          |                  | <0.5                      |                  | 6.9                       |                  | 1649                                      | 119 / 34 / 111              |                        |
| 34    |              | 6150 <sup>e</sup>          |                  | 4630 <sup>e</sup>          |                  | 390 <sup>e</sup>          |                  | 17.7                      |                  | 1432                                      | >120 / 77 / >120            |                        |

<sup>a</sup>Data are the geometric mean of two independent experiments ( $n = 2$ ) unless otherwise specified. Assay details reported in [Supporting Information](#). <sup>b</sup>Permeability ( $P_{app} \times 10^{-6}$  cm/s) as measured in PAMPA assay. <sup>c</sup>Half-life of compound incubated with rat (R), mouse (M), or human (H) liver microsomes (LM). <sup>e</sup>Data are from a single experiment ( $n = 1$ ).

Key compounds displayed potent block of IRAK1/4-mediated signaling in a cellular NF- $\kappa$ B assay ([Table 5](#)). In this assay, signaling was initiated at either the TLR2 or IL1R receptors using Pam3SCK4 or IL1B, respectively. That signaling proceeds through IRAK1 and IRAK4 and results in production of NF- $\kappa$ B. Compounds **27**, **30**, and **36** all showed potent inhibition of NF- $\kappa$ B production, and thus potent block of signaling through the IRAK1/4 mediated pathway, when signaling was initiated with either Pam3SCK4 or IL1B.

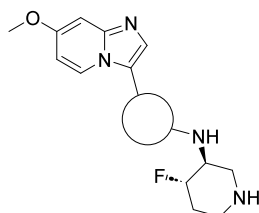
Finally, compounds **27**, **30**, and **36** potently inhibited the growth of AML tumor cells. As shown in [Table 5](#), these compounds all potently inhibited the growth of MOLM14 tumor cells that contained FLT3 (D835Y) or (F691L) mutations. These data suggest that compounds **27**, **30**, and **36** could prove efficacious in *in vivo* settings as treatments for cancers that harbor these mutations.

In Western blot experiments employing THP1 or MOLM14 (D835Y) cells, compounds **27**, **30** and **36** inhibited phosphorylation of IRAK or FLT3 substrates at concentrations similar to their IC<sub>50</sub>s in the NF- $\kappa$ B or MOLM14 (D835Y) assays (see [Supporting Information Figure S2](#) for details).

Compounds **27**, **30**, and **36** exhibited little or no activity when tested versus a panel of cardiac ion channels and cytochrome P450 (CYP) enzymes. As shown in [Table 6](#), these compounds displayed moderate block of hERG, but no appreciable block of Na<sub>v</sub>1.5 or Ca<sub>v</sub>1.2 at concentrations up to 30 μM. Compounds **27** and **30** displayed modest inhibition of CYP2D6, but no significant inhibition of six other CYP isoforms. Similarly, compound **36** evinced moderate inhibition of CYP2C9 and CYP2D6, but no significant inhibition of the other five CYP isoforms tested.

Compounds **27**, **30**, and **36** selectively inhibited key targets relative to other kinases. These compounds were initially tested

Table 4. Effect of Central Ring on Potency, hERG, and In Vitro ADME Properties



| Compd | Central Ring | IRAK1 IC <sub>50</sub> (nM) <sup>a</sup> | IRAK4 IC <sub>50</sub> (nM) <sup>a</sup> | FLT3 IC <sub>50</sub> (nM) <sup>a</sup> | hERG IC <sub>50</sub> (μM) <sup>a</sup> | PAMPA (P <sub>app</sub> ) <sup>b</sup> | R/M/H LM t <sub>1/2</sub> (min) <sup>d</sup> |
|-------|--------------|--|--|---|---|--|--|
| 35    |              | 9  | <0.5                                     | <0.5                                    | 3.7                                     | 1423                                   | >120 / 91 / 37                               |
| 36    |              | 11                                       | 0.5                                      | <0.5                                    | 20.5                                    | 220                                    | >120 / 42 / >120                             |
| 37    |              | 4  | <0.5                                     | <0.5                                    | 6.5                                     | 881                                    | >120 / >120 / 86                             |
| 38    |              | 89 <sup>e</sup>                          | 25 <sup>e</sup>                          | 1 <sup>e</sup>                          | N.D.                                    | 1607                                   | 26 / 12 / 21                                 |

<sup>a</sup>Data are the geometric mean of two independent experiments ( $n = 2$ ) unless otherwise specified. Assay details reported in Supporting Information. <sup>b</sup>Permeability ( $P_{app} \times 10^{-6}$  cm/s) as measured in PAMPA assay. <sup>d</sup>Half-life of compound incubated with rat (R), mouse (M), or human (H) liver microsomes (LM). <sup>e</sup>Data are from a single experiment ( $n = 1$ ).

Table 5. Cellular Potencies of Key Compounds

|  | 27   | 30              | 36              |
|--|------|-----------------|-----------------|
| NanoBRET IRAK4 IC <sub>50</sub> (nM) <sup>a</sup>        | <0.5 | <0.5            | 1               |
| NanoBRET FLT3 IC <sub>50</sub> (nM) <sup>a</sup>         | 0.8  | 0.8             | 71              |
| NanoBRET FLT3 (D835Y) IC <sub>50</sub> (nM) <sup>a</sup> | <0.5 | N.D.            | <0.5            |
| NF-κB (Pam3SCK4) IC <sub>50</sub> (nM) <sup>b</sup>      | 16   | 25              | 16              |
| NF-κB (IL1B) IC <sub>50</sub> (nM) <sup>b</sup>          | 25   | 35              | 17              |
| MOLM14 (D835Y) IC <sub>50</sub> (nM) <sup>c</sup>        | 15   | 18 <sup>d</sup> | 20 <sup>e</sup> |
| MOLM14 (F691L) IC <sub>50</sub> (nM) <sup>b</sup>        | 139  | 85              | 55 <sup>f</sup> |

<sup>a</sup>Data are the geometric mean of two independent experiments ( $n = 2$ ). <sup>b</sup>Data are the geometric mean of two independent experiments ( $n = 2$ ) unless otherwise specified. <sup>c</sup>Data are the geometric mean of three independent experiments ( $n = 3$ ) unless otherwise specified. <sup>d</sup>Data are the geometric mean of four independent experiments ( $n = 4$ ). <sup>e</sup>Data are the geometric mean of two independent experiments ( $n = 2$ ). <sup>f</sup>Data are from a single experiment ( $n = 1$ ).

Table 6. Off-Target Activities of Key Compounds

|  | 27  | 30  | 36               |
|--|-----|-----|------------------|
| hERG IC <sub>50</sub> (μM) <sup>a</sup>                | 6.7 | 5.1 | 20.5             |
| Na <sub>v</sub> 1.5 IC <sub>50</sub> (μM) <sup>a</sup> | >30 | >30 | >30              |
| Ca <sub>v</sub> 1.2 IC <sub>50</sub> (μM) <sup>a</sup> | >30 | >30 | >30              |
| CYP3A4 IC <sub>50</sub> (μM) <sup>a</sup>              | >25 | >25 | >25 <sup>b</sup> |
| CYP2C9 IC <sub>50</sub> (μM) <sup>a</sup>              | >25 | >25 | 4 <sup>b</sup>   |
| CYP2D6 IC <sub>50</sub> (μM) <sup>a</sup>              | 15  | 8   | 12 <sup>b</sup>  |
| CYP1A2 IC <sub>50</sub> (μM) <sup>b</sup>              | >25 | >25 | >25              |
| CYP2B6 IC <sub>50</sub> (μM) <sup>b</sup>              | >25 | >25 | >25              |
| CYP2C8 IC <sub>50</sub> (μM) <sup>b</sup>              | >25 | >25 | >25              |
| CYP2C19 IC <sub>50</sub> (μM) <sup>b</sup>             | >25 | >25 | >25              |

<sup>a</sup>Data are the geometric mean of two independent experiments ( $n = 2$ ) unless otherwise specified. <sup>b</sup>Data are from a single experiment ( $n = 1$ ).

for inhibition of a representative set of 50 kinases (see Supporting Information Tables S3–S5 for details). From this set, 27 displayed significantly higher kinase selectivity than 30 or

36. Compound 27 was then further profiled for inhibition of a larger set of 370 wild-type kinases. As shown in Figure 3, relative

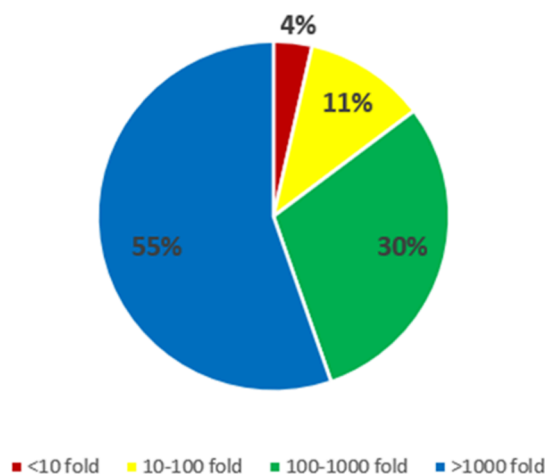


**Figure 3.** Kinase selectivity profile of compound 27. For each off-target kinase, selectivity was calculated vs IRAK4 and represented as fold selectivity (IC<sub>50</sub> of off-target kinase/IC<sub>50</sub> IRAK4). Percentages refer to percent of 370 kinase panel.

to its inhibition of IRAK4, compound 27 displayed >100-fold selectivity vs 85% of the 370 kinase panel. Compound 27 thus displays improved kinase selectivity relative to key compounds from this series reported previously, and high kinase selectivity overall.

Select compounds were profiled in rat pharmacokinetic (PK) experiments (Table 7). Compound 23, the parent compound for this series, displayed high oral bioavailability and moderate oral exposure (AUC), but suffered from a high rate of plasma clearance. Compounds 30 and 36 exhibited similarly high rates of plasma clearance as well as lower oral bioavailability and oral exposure. Compound 27 displayed the best overall PK profile in this series, one that features lower clearance, higher oral

Table 7. In Vitro ADME and In Vivo Pharmacokinetic Properties of Select Compounds

| compd | species | cLog D | In Vitro ADME  |   |                              | In Vivo PK <sup>d</sup> |          |  |                                |                         |
|-------|---------|--------|--|---|------------------------------|-------------------------|----------|--|--------------------------------|-------------------------|
|       |         |        | LM Cl <sub>int</sub> <sup>a</sup><br>( $\mu\text{L}/\text{min}$ ) <sup>a</sup> | Hep Cl <sub>int</sub> <sup>b</sup><br>( $\mu\text{L}/\text{min}$ ) <sup>b</sup> | PPB<br>(% free) <sup>c</sup> | Dose (iv/po)<br>(mg/kg) | F<br>(%) | AUC (po)<br>( $\mu\text{M}\cdot\text{h}$ ) | Cl <sub>p</sub><br>(mL/min/kg) | t <sub>1/2</sub><br>(h) |
| 23    | rat     | 1.9    | <12  | 21  | 4.8                          | 1/3                     | 70       | 1.91                                       | 50                             | 3.6                     |
| 30    | rat     | 1.7    | 13   | 13  | 11.2                         | 1/3                     | 21       | 0.51                                       | 56                             | 1.8                     |
| 36    | rat     | 0.7    | <12  | 34  | 16.1                         | 1/3                     | 30       | 0.98                                       | 67                             | 2.1                     |
| 27    | rat     | 2.1    | 17   | 32  | 2.2                          | 1/3                     | 64       | 2.43                                       | 33                             | 5.0                     |
| 27    | mouse   | 2.1    | 34   | 68  | 3.0                          | 1/3                     | 64       | 1.63                                       | 52                             | 5.5                     |

<sup>a</sup>Intrinsic clearance rate in liver microsomes ( $\mu\text{L}/\text{min}/\text{mg}$  protein). <sup>b</sup>Intrinsic clearance in hepatocytes ( $\mu\text{L}/\text{min}/10^6$  cells). <sup>c</sup>Plasma protein binding, expressed as percent free (unbound) compound. <sup>d</sup>See Supporting Information for PK experiment details.

exposure, and a longer half-life relative to those observed for compounds 23, 30 or 36.

The pharmacokinetic profile of compound 27 was also examined in mouse. As shown in Table 7, 27 displayed a mouse PK profile that was broadly similar to its profile in rat, albeit with slightly higher clearance and concomitantly lower oral exposure.

Compound 27 was selected for testing in a mouse xenograft model of AML. In this study, we anticipated testing several compounds in experiments that would collectively require dosing 70 mice per day for up to 60 days. Although compound 27's mouse PK profile permitted oral dosing, intraperitoneal (IP) dosing was considered a more practical choice given the large volume of dosing expected. The xenograft studies were thus conducted using IP dosing with PK monitored in a separate study arm.

In a mouse xenograft model of AML, compound 27 produced survival prolongation superior to that of gilteritinib, the leading FDA-approved FLT3 inhibitor currently used to treat AML. In this model, NSG-SGM3 mice were intravenously xenografted with MOLM14 AML tumor cells that contained clinically important FLT3 (D835Y) and (ITD) mutations. Compound dosing was initiated 21 days following engraftment. Mice were dosed once daily Monday–Friday with either vehicle (PBS), 10 mg/kg IP gilteritinib, or 10 mg/kg IP compound 27 (n = 10 mice per dosing arm).<sup>14</sup> As shown in Figure 4, mice dosed with

In a separate PK arm of the study, NSG-SGM3 mice were dosed once daily Monday through Friday with 10 mg/kg IP compound 27. Blood samples were collected 1 h postdose on dosing days 1, 5, 22 and 26, and 4 h postdose on day 5. The unbound plasma concentrations of compound 27 1 h postdose ranged from 41 to 66 nM, or roughly 3–4 $\times$  above the compound's MOLM14 (D835Y) IC<sub>50</sub> (15 nM). On day 5, the unbound plasma concentration of 27 was 39 nM at 4 h postdose, or 2–3 $\times$  above the target IC<sub>50</sub>. The unbound plasma concentrations of gilteritinib were similar, and ranged from 41 to 146 nM 1 h postdose. Thus, at equivalent doses, and at similar concentrations, compound 27 produced survival prolongation superior to that of gilteritinib.

In summary, we have reported herein the optimization of a series of IRAK-FLT3 inhibitors. Key compound 27 from this series displays potent and selective inhibition of IRAK1, IRAK4, and FLT3, reduced block of hERG, good ADME and PK properties, and efficacy superior to that of gilteritinib in a mouse xenograft model of AML. Further optimization in this series is ongoing, and will be reported in due course.

## ■ ASSOCIATED CONTENT

### Supporting Information

The Supporting Information is available free of charge at <https://pubs.acs.org/doi/10.1021/acsmchemlett.5c00147>.

Synthesis procedures and characterization data for compounds 2–15, 17–23, and 27–34; kinase selectivity data for compounds 27, 30, and 36; procedures for functional biochemical assays, binding assays, NanoBRET assays, NF- $\kappa$ B assays, MOLM14 cell viability assays, in vitro ADME assays, pharmacokinetic assays, and mouse xenograft assay (PDF)

## ■ AUTHOR INFORMATION

### Corresponding Author

Scott B. Hoyt – National Center for Advancing Translational Sciences, Rockville, Maryland 20850, United States;  
[orcid.org/0009-0009-9788-1935](https://orcid.org/0009-0009-9788-1935); Email: [scott.hoyt@nih.gov](mailto:scott.hoyt@nih.gov)

### Authors

Chris J. Finocchio – National Center for Advancing Translational Sciences, Rockville, Maryland 20850, United States  
 Elizabeth Croll – National Center for Advancing Translational Sciences, Rockville, Maryland 20850, United States  
 Gregory J. Tawa – National Center for Advancing Translational Sciences, Rockville, Maryland 20850, United States

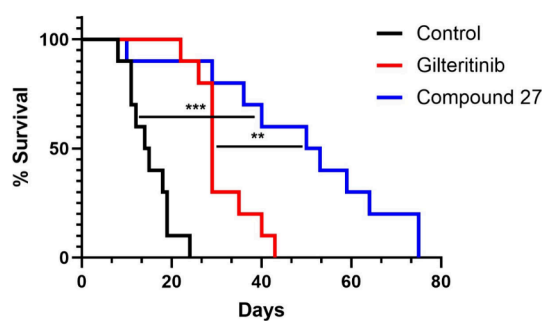


Figure 4. Kaplan–Meier survival analysis of NSGS mice engrafted with MOLM14 (ITD, D835Y) cells and treated with compound 27 or gilteritinib.

vehicle survived for a median of 15 days from the start of dosing, while mice dosed with the positive control gilteritinib survived for a median of 29 days. In comparison, mice dosed with compound 27 survived significantly longer (median 52 days) than those dosed with either vehicle or gilteritinib. In each case, the difference in median survival time was statistically significant (log-rank test,  $P = 0.0001$  for 27 vs vehicle;  $P = 0.004$  for 27 vs gilteritinib).

**Mingliang Zhang** – WuXi AppTec Co. Ltd., Tianjin 300457, People's Republic of China  
**Jiangong Wang** – WuXi AppTec Co. Ltd., Tianjin 300457, People's Republic of China  
**Huixi Li** – WuXi AppTec Co. Ltd., Tianjin 300457, People's Republic of China  
**Li Ma** – WuXi AppTec Co. Ltd., Tianjin 300457, People's Republic of China  
**Kaikai Li** – WuXi AppTec Co. Ltd., Tianjin 300457, People's Republic of China  
**Xiaohu Zhang** – National Center for Advancing Translational Sciences, Rockville, Maryland 20850, United States  
**Xin Xu** – National Center for Advancing Translational Sciences, Rockville, Maryland 20850, United States  
**Pranav Shah** – National Center for Advancing Translational Sciences, Rockville, Maryland 20850, United States  
**Yuhong Fang** – National Center for Advancing Translational Sciences, Rockville, Maryland 20850, United States  
**Lyndsey C. Bolanos** – Cincinnati Children's Hospital Medical Center, Division of Experimental Hematology, Cincinnati, Ohio 45229, United States  
**Gabriel Gracia-Maldonado** – Kurome Therapeutics, Cincinnati, Ohio 45208, United States  
**Amal Kolt** – Kurome Therapeutics, Cincinnati, Ohio 45208, United States  
**Christina Robinson** – Frederick National Laboratory for Cancer Research, Frederick, Maryland 21702, United States  
**Jessica Free** – Frederick National Laboratory for Cancer Research, Frederick, Maryland 21702, United States  
**Elijah F. Edmondson** – Frederick National Laboratory for Cancer Research, Frederick, Maryland 21702, United States; [orcid.org/0000-0002-6106-3705](https://orcid.org/0000-0002-6106-3705)  
**Simone Diflippantonio** – Frederick National Laboratory for Cancer Research, Frederick, Maryland 21702, United States  
**LaQuita M. Jones** – Cincinnati Children's Hospital Medical Center, Division of Oncology, Cincinnati, Ohio 45229, United States  
**Ashley E. Culver-Cochran** – Cincinnati Children's Hospital Medical Center, Division of Experimental Hematology, Cincinnati, Ohio 45229, United States  
**Jan S. Rosenbaum** – Kurome Therapeutics, Cincinnati, Ohio 45208, United States  
**Daniel T. Starczynowski** – Cincinnati Children's Hospital Medical Center, Division of Experimental Hematology, Cincinnati, Ohio 45229, United States  
**Craig J. Thomas** – National Center for Advancing Translational Sciences, Rockville, Maryland 20850, United States; National Cancer Institute, Bethesda, Maryland 20814, United States; [orcid.org/0000-0001-9386-9001](https://orcid.org/0000-0001-9386-9001)

Complete contact information is available at:  
<https://pubs.acs.org/10.1021/acsmmedchemlett.5c00147>

### Author Contributions

The manuscript was written by S.B.H. with contributions from all authors.

### Funding

This work was supported in part by NIH (U54DK126108, R35HL135787, R01CA275007), Cincinnati Children's Hospital Research Foundation, and Cancer Free Kids grants to D.T.S., and by NCATS grant 1ZIATR000044. This project has been funded in whole or in part with Federal funds from the National Cancer Institute, National Institutes of Health, under Contract

No. HHSN261201500003I. The content of this publication does not necessarily reflect the views or policies of the Department of Health and Human Services, nor does mention of trade names, commercial products, or organizations imply endorsement by the U.S. Government. This contract number represents work performed within the scope of work of the nonseverable IDIQ contract.

### Notes

No unexpected or unusually high safety hazards were encountered.

The authors declare the following competing financial interest(s): D.T.S. serves on the scientific advisory board at Kurome Therapeutics, is a consultant for and/or received funding from Kurome Therapeutics, Captor Therapeutics, Treeline Biosciences, and Tolerio Therapeutics, and has equity in Kurome Therapeutics. L.C.B. consulted for Kurome Therapeutics. J.R. is employed by and holds equity in Kurome Therapeutics, holds equity in Airway Therapeutics, and is a consultant for Radius Health and MoglingBio. G.G.-M. was employed by and holds equity in Kurome Therapeutics. A.K. is employed by and holds equity in Kurome Therapeutics. S.B.H. and C.J.T. are inventors on patent WO 2022026935. Their rights have been assigned to the U.S. government, but they may receive royalties on the patent.

### ACKNOWLEDGMENTS

The authors thank Nishita Rao, Shane Biesecker, and Chris LeClair for their assistance with compound purification.

### ABBREVIATIONS

ADME, absorption, distribution, metabolism, and elimination; AML, acute myeloid leukemia; BRET, bioluminescence resonance energy transfer; CYP, cytochrome P450; EWG, electron-withdrawing group; FLT3, FMS-like tyrosine kinase 3; hERG, human Ether-a-go-go-Related Gene; IRAK1, interleukin 1 receptor associated kinase 1; IRAK4, interleukin 1 receptor associated kinase 4; ITD, internal tandem duplication; NF- $\kappa$ B, nuclear factor kappa B; PAMPA, parallel artificial membrane permeability assay; PK, pharmacokinetic; SAR, structure–activity relationship

### REFERENCES

- (1) Dohner, H.; Wei, A. H.; Lowenberg, B. Towards precision medicine for AML. *Nat. Rev. Clin. Oncol.* **2021**, *18*, 577–590.
- (2) Levis, M.; Perl, A. E. Gilteritinib: potent targeting of FLT3 mutations in AML. *Blood Adv.* **2020**, *4*, 1178–1191.
- (3) National Cancer Institute (NIH–NCI) Website. <https://seer.cancer.gov/statfacts/html/amyl.html> (accessed 2023-10-06).
- (4) Zhong, Y.; Qiu, R.-Z.; Sun, S.-L.; Zhao, C.; Fan, T.-Y.; Chen, M.; Li, N.-G.; Shi, Z.-H. Small-molecule Fms-like tyrosine kinase 3 inhibitors: an attractive and efficient method for the treatment of acute myeloid leukemia. *J. Med. Chem.* **2020**, *63*, 12403–12428.
- (5) Kennedy, V. E.; Smith, C. C. FLT3 mutations in acute myeloid leukemia: key concepts and emerging controversies. *Front. Oncol.* **2020**, *10*, No. 612880.
- (6) Knight, T. E.; Edwards, H.; Meshinchi, S.; Taub, J. W.; Ge, Y. “FLipping” the story: FLT3-mutated acute myeloid leukemia and the evolving role of FLT3 inhibitors. *Cancers* **2022**, *14*, 3398–3423.
- (7) Acharya, B.; Saha, D.; Armstrong, D.; Lakkaniga, N. R.; Frett, B. FLT3 inhibitors for acute myeloid leukemia: successes, defeats, and emerging paradigms. *RSC Med. Chem.* **2022**, *13*, 798–816.
- (8) Melgar, K.; Walker, M. M.; Jones, L. M.; Bolanos, L. C.; Hueneman, K.; Wunderlich, M.; Jiang, J.-K.; Wilson, K. M.; Zhang, X.; Sutter, P.; Wang, A.; Xu, X.; Choi, K.; Tawa, G.; Lorimer, D.;

Abendroth, J.; O'Brien, E.; Hoyt, S. B.; Berman, E.; Famulare, C. A.; Mulloy, J. C.; Levine, R. L.; Perentesis, J. P.; Thomas, C. J.; Starczynowski, D. T. Overcoming adaptive therapy resistance in AML by targeting immune response pathways. *Sci. Transl. Med.* **2019**, *11*, No. eaaw8828.

(9) Bennett, J.; Ishikawa, C.; Agarwal, P.; Yeung, J.; Sampson, A.; Uible, E.; Vick, E.; Bolanos, L. C.; Hueneman, K.; Wunderlich, M.; Kolt, A.; Choi, K.; Volk, A.; Greis, K. D.; Rosenbaum, J.; Hoyt, S. B.; Thomas, C. J.; Starczynowski, D. T. Paralog-specific signaling by IRAK1/4 maintains MyD88-independent functions in MDS/AML. *Blood* **2023**, *142*, 989–1007.

(10) Hoyt, S. B.; Finocchio, C. J.; Croll, E.; Tawa, G. J.; Li, H.; Ma, L.; Li, K.; Liu, L.; Li, R.; Zhang, X.; Wilson, K.; Xu, X.; Shah, P.; Williams, J.; Bolanos, L. C.; Gracia-Maldonado, G.; Kolt, A.; Robinson, C.; Free, J.; Edmondson, E. F.; Difilippantonio, S.; Rosenbaum, J. S.; Starczynowski, D. T.; Thomas, C. J.; et al. Discovery of IRAK1/4/pan-FLT3 kinase inhibitors as treatments for acute myeloid leukemia. *ACS Med. Chem. Lett.* **2024**, *15*, 1843–1851.

(11) Cavalli, A.; Poluzzi, E.; De Ponti, F.; Recanatini, M. Toward a pharmacophore for drugs inducing the long QT syndrome: insights from a CoMFA study of hERG K<sup>+</sup> channel blockers. *J. Med. Chem.* **2002**, *45*, 3844–3853.

(12) Garrido, A.; Lepailleur, A.; Mignani, S. M.; Dallemagne, P.; Rochais, C. hERG toxicity assessment: useful guidelines for drug design. *Eur. J. Med. Chem.* **2020**, *195*, 112290.

(13) As described in the [Supporting Information](#), our PAMPA assay incorporates stirring, resulting in higher  $P_{app}$  values than nonstirred models. In this assay,  $P_{app} < 10$  indicates low permeability,  $P_{app} = 10–100$  indicates moderate permeability, and  $P_{app} > 100$  indicates high permeability.

(14) Mice were not dosed on weekends for logistical/staffing reasons.